Transmembrane Helices 3 and 4 Are Involved in Substrate Recognition by the Na^+/Dicarboxylate Cotransporter, NaDC1[†]

Naomi Oshiro,[‡] Steven C. King,[§] and Ana M. Pajor*,[‡]

Department of Biochemistry and Molecular Biology, University of Texas Medical Branch, Galveston, Texas 77555-0645, and Department of Integrative Biosciences, Oregon Health & Science University, Portland, Oregon 97239-3097

Received November 14, 2005; Revised Manuscript Received December 22, 2005

ABSTRACT: The Na^+/dicarboxylate cotransporters (NaDC1) from mouse (m) and rabbit (rb) differ in their ability to handle glutarate. Substrate-dependent inward currents, measured using two-electrode voltage clamp, were similar for glutarate and succinate in *Xenopus* oocytes expressing mNaDC1. In contrast, currents evoked by glutarate in rbNaDC1 were only about 5% of the succinate-dependent currents. To identify domains involved in glutarate transport, we constructed a series of chimeric transporters between mouse and rabbit NaDC1. Although residues found in multiple transmembrane helices (TM) participate in glutarate transport, the most important contribution is made by TM 3 and 4 and the associated loops. The R(M3−4) chimera, consisting of rbNaDC1 with substitution of TM 3−4 from mNaDC1, had a decreased $K_{0.5}^{\text{glutarate}}$ of 4 mM compared with 15 mM in wild-type rbNaDC1 without any effect on $K_{0.5}^{\text{succinate}}$. The chimeras were also characterized using dual-label competitive uptakes with ^{14}C-glutarate and ^{3}H-succinate to calculate the transport specificity ratio (TSR), a measure of relative catalytic efficiency with the two substrates. The TSR analysis provides evidence for functional coupling in the transition state between TM 3 and 4. We conclude that TM 3 and 4 contain amino acid residues that are important determinants of substrate specificity and catalytic efficiency in NaDC1.

The active transport of citric acid cycle intermediates, such as succinate and citrate, across plasma membranes occurs on Na^+/dicarboxylate cotransporters (NaDCs[1]) belonging to the SLC13 gene family (*1*). The low-affinity NaDC1 transporter is found in brush border membranes of renal proximal tubules and the gastrointestinal tract (*2*). The physiological function of NaDCs includes absorption of dietary di- and tricarboxylates and participation in organic anion secretion by contributing dicarboxylates to the organic anion/dicarboxylate exchangers (*3*). In the kidney, NaDC1 helps to regulate the concentration of urinary citrate which affects the development of kidney stones (*4*). The NaDCs have also been implicated in longevity since mutations in the genes coding for dicarboxylate transporter homologs from *Drosophila* and *Caenorhabditis elegans* produce increases in lifespan (*5*, *6*).

The current secondary structure model of NaDC1 contains 11 transmembrane helices (TM) with an intracellular N-terminus and an extracellular C-terminus (*7*, *8*). Residues involved in determining differences in substrate affinity and cation selectivity are found in the C-terminal half of the protein although the first four TMs also affect substrate binding affinity, sensitivity to inhibitors, and cation selectivity (*9*−*11*). NaDC1 generally prefers four-carbon dicarboxylate substrates, such as succinate (*12*). However, NaDC1 from mouse exhibits functional properties that differ from those of the rabbit or human NaDC1. The mNaDC1 substrate specificity resembles that of the high affinity NaDC3 transporters, including the ability to transport longer or bulkier dicarboxylates such as glutarate and 2,3-dimethylsuccinate in addition to succinate (*13*, *14*). To date, the amino acids or domains responsible for these functional differences between NaDC1 orthologs have not been identified.

This study was undertaken to identify domains responsible for differences in glutarate selectivity in the NaDC transporters. We compared mouse and rabbit NaDC1, which have a high sequence identity of 75% but differences in handling of glutarate (*13*). The results of this study show that residues from multiple TMs are involved in glutarate transport, with TM 3 and 4 and associated loops contributing most to the total glutarate-induced inward currents. Furthermore, we find evidence of functional interaction in the transition state between amino acids in TM 3 and TM 4.

EXPERIMENTAL PROCEDURES

Nomenclature of Chimeric and Mutant transporters. The chimeric transporters constructed with mouse (m) NaDC1 (GenBank AF201903) and rabbit (rb) NaDC1 (GenBank U12186) are designated using the letters M (mouse) and R (rabbit) following the number of transmembrane helices (TM) that are contributed by mNaDC1 at the amino terminus. For example, 2MR contains TM 1−2 of mNaDC1 and the rest

---

[†] This study was supported by National Institute of Health Grants DK46269 (to A.M.P.) and NS38226 (to S.C.K.).

* Author for correspondence: Department of Biochemistry and Molecular Biology, University of Texas Medical Branch, Galveston, TX 77555-0645. Telephone: 409-772-3434. Fax: 409-772-5102. E-mail: ampajor@utmb.edu.

[‡] University of Texas Medical Branch.

[§] Oregon Health & Science University.

[1] Abbreviations: mNaDC1, mouse Na^+/dicarboxylate cotransporter 1; rbNaDC1, rabbit Na^+/dicarboxylate cotransporter 1; TM, transmembrane helix; TSR, transport specificity ratio

10.1021/bi052328g CCC: $33.50
Published on Web 01/25/2006

from rbNaDC1. The mutant transporters are named using the single letter amino acid code followed by the number of the position that was mutated. The second letter following the sequence number shows the amino acid substituted at that position. The numbering of amino acid sequence is based on the mNaDC1 sequence.

Site-Directed Mutagenesis. Restriction enzyme sites for preparing chimeras were introduced by silent mutagenesis into intracellular and extracellular loops of mNaDC1 and rbNaDC1. A few of the initial mutants in this study were made using the oligonucleotide-directed Kunkel method (*15*), but most of the mutants were made using the QuikChange site-directed mutagenesis kit (Stratagene) according to the manufacturer's directions. Briefly, the parental double-stranded cDNA was heat denatured and annealed with both sense and anti-sense oligonucleotides containing the desired mutations. The parental cDNA was cut with *Dpn*I, and the undigested cDNA incorporating the mutations was transformed into the XL-1 blue strain of *Escherichia coli*. All of the mutants were verified by sequencing at the Protein Chemistry Laboratory of the University of Texas Medical Branch.

Construction of Chimeric Transporter cDNAs. Chimeric transporter cDNAs containing portions of mouse and rabbit NaDC1 cDNAs were constructed by subcloning using endogenous or introduced restriction enzyme sites. The junctions of the chimeras were located in loops outside of putative TMs. The numbering of the junctions is based on the mNaDC1 amino acid sequence, and the equivalent positions in rbNaDC1 were selected to avoid additional mutations in the chimeras. The 2MR chimera was constructed using an introduced *Hind*III site at amino acid position 74 in mNaDC1 and the endogenous *Hind*III site in rbNaDC1. The 4MR chimera was created by using the endogenous *Sac*I sites at position 177. For the 3MR and 6−10MR chimeras, junctions at amino acid 120 (*Ngo*MIV), 284 (*Avr*II), 341 (*Nru*I), 427 (*Nru*I), 489 (*Nde*I), and 518 (*Bsm*I), respectively, were made by introducing restriction enzyme sites. The junctions to construct TM 3 and TM 4 chimeras, R(M3) and R(M4), were the same as those for 2MR, 3MR, and 4MR. All of the chimeras were confirmed by sequencing at the Protein Chemistry Laboratory of the University of Texas Medical Branch.

Xenopus Oocyte Injections. The cDNAs of wild-type, chimeras, and mutant NaDC1 were linearized at the *Xba*I site in the pSPORT1 vector and used as templates for *in vitro* transcription using the T7 mMessage mMachine kit (Ambion). The cRNA was stored at −80 °C until use. Female *Xenopus laevis* were either purchased from Xenopus I or donated by Dr. Cheryl Watson. Stage V and VI oocytes were dissected and treated with collagenase as described previously (*16*) or by using a modified protocol in which oocytes were incubated for 3 h with 2 mg/mL collagenase without the subsequent phosphate buffer treatment. The defolliculated oocytes were injected with 46−50 nL of cRNA the day after dissection and cultured at 18 °C in Barth's medium supplemented with 5% heat-inactivated horse serum, 2.5 mM pyruvate, 100 μg/mL gentamycin sulfate, and either 50 μg/mL tetracycline or a mixture of 5 μg/mL ceftazidime (GlaxoSmithKline) and 100 units/mL penicillin−100 μg/mL streptomycin (Gibco). Experiments were done 3 to 6 days following injection. Culture vials and medium were changed daily.

Electrophysiology. Oocytes expressing each wild-type, chimera, and mutant NaDC1 transporter were used to measure substrate-induced inward currents using the two-electrode voltage clamp (TEVC) method as described previously (*12*, *17*). The 100 ms test pulses were configured by the pClamp6 program (Axon instruments, Inc.) between +50 and −150 mV in decrements of 20 mV. The membrane potential was held at −50 mV between trials, and the average of three measurements was taken for every trial. The electrode resistance was less than 0.5 MΩ.

Oocytes were first equilibrated in choline buffer containing 100 mM choline chloride, 2 mM KCl, 1 mM $MgCl_2$, 1 mM $CaCl_2$, and 10 mM HEPES, pH adjusted to 7.5 with 1 M Tris. This was followed by sodium buffer containing 100 mM NaCl instead of choline chloride. The test solutions of 1 mM substrates in sodium buffer were then added, and the voltage pulse protocol was initiated. The substrate was washed away using choline buffer, and subsequent experiments were conducted after recovery of basal currents. Substrate-induced currents were calculated from the difference between steady-state currents in the presence and absence of substrate. The kinetic data were analyzed using SigmaPlot software (Jandel Scientific). The steady-state substrate-induced currents were fitted to the Michaelis−Menten equation:

$$I = I_{max}\frac{[S]}{K_{0.5} + [S]} \tag{1}$$

where I is the current, I_{max} is the maximum current at saturating substrate concentration, [S] is the substrate concentration, and $K_{0.5}$ is the substrate concentration that produces half I_{max}. Statistical analysis was performed using the SigmaStat program (Jandel Scientific). Experiments were repeated with oocytes from at least two to four different frogs.

Dual-Label Competitive Transport Assay and Transport Specificity Ratio (TSR). Transport solutions were prepared in sodium buffer containing a mixture of 150 μM ^{14}C-glutarate (American Radiolabeled Chemicals, Inc) and 50 μM ^{3}H-succinate (ViTrax Co.). In the transport assays, oocytes were rinsed with choline buffer to remove sodium and serum as described (*16*). Transport was initiated by replacing choline buffer with 0.4 mL of the transport solution. The uptake reaction was stopped by adding 4 mL of ice-cold choline buffer followed by three washes with cold choline buffer to remove extracellular radioactivity. Individual oocytes were transferred to scintillation vials and dissolved in 0.25 mL of 10% SDS. Radioactivity of the samples was measured by dual-label scintillation counting. Counts in uninjected oocytes were subtracted from counts obtained in cRNA-injected oocytes.

The transport specificity ratio (TSR) is a constant that reflects a difference in substrate affinities for two competing substrates in their transition states of carrier−substrate complexes (*18*). Experimentally, the TSR is determined from the initial rates (v) of a competitive transport reaction with both ^{3}H-succinate and ^{14}C-glutarate and the concentrations of the substrates using the following equation:

$$\mathrm{TSR} = \left(\frac{v_{\mathrm{glutarate}}}{v_{\mathrm{succinate}}}\right)\left(\frac{[\mathrm{succinate}]}{[\mathrm{glutarate}]}\right) \quad (2)$$

The TSR is an expression-independent constant that provides information on the change in binding energy ($\Delta\Delta G_b$) resulting from structural differences between the two competing substrates, in this case succinate and glutarate, as given in the following equation (From (*18*)):

$$\mathrm{TSR} = \frac{\left(\dfrac{k_{\mathrm{cat}}}{K_{\mathrm{m}}}\right)_{\mathrm{glutarate}}}{\left(\dfrac{k_{\mathrm{cat}}}{K_{\mathrm{m}}}\right)_{\mathrm{succinate}}} = \exp(-\Delta\Delta G_b/RT) \quad (3)$$

where R and T refer to the gas constant (8.31 J/K/mol) and temperature (296 K), respectively. A change in TSR value indicates a change in the transition binding energy of at least one of the two substrates. Changes in free energy associated with the single and double chimeras involving TM 3 and 4 were calculated using the following equation (*19*):

$$\Delta(\Delta\Delta G_b) = -RT \ln\left[\frac{\mathrm{TSR}_{\mathrm{chimera}}}{\mathrm{TSR}_{\mathrm{wild-type}}}\right] \quad (4)$$

RESULTS

Voltage-Dependent Currents in Mouse and Rabbit NaDC1. Glutarate and succinate are dicarboxylic acids that differ in length by only one carbon. Our previous experiments using radiotracer uptakes and two-electrode voltage clamp measurements indicated that the mouse and rabbit NaDC1 exhibit differences in their ability to transport glutarate (*12*, *13*, *20*). Those findings were verified and extended in this study. As shown in Figure 1, mNaDC1 exhibited large voltage-dependent inward currents with both glutarate and succinate. In contrast, rbNaDC1 exhibited inward currents in the presence of succinate, but only very small currents with glutarate.

Glutarate Kinetics in Oocytes Expressing mNaDC1 and rbNaDC1. We next examined the kinetics for glutarate in mNaDC1 and rbNaDC1. The steady-state currents induced by increasing concentrations of glutarate at −50 mV are shown in Figure 2. In the single experiment shown in Figure 2A, the $K_{0.5}$ for glutarate in mNaDC1 was 194 μM, and the $I_{\max}$ was −386 nA. In three experiments, the mean $K_{0.5}{}^{\mathrm{glutarate}}$ was 252 ± 100 μM (mean ± SEM), and the $I_{\max}{}^{\mathrm{glutarate}}$ was −476 ± 112 nA. The kinetics of glutarate were more difficult to measure in rbNaDC1 because the currents were very small at low concentrations, but in a single experiment the $K_{0.5}$ for glutarate was approximately 15 mM, and the $I_{\max}$ was −289 nA (Figure 2B). For comparison, the K_{m} for glutarate in rbNaDC1 was 7 mM measured using radiotracer (*20*). The succinate $K_{0.5}$ values were only about 2-fold different in the two transporters with a mean $K_{0.5}$ in mNaDC1 of 99 ± 15 μM (mean ± SEM, n = 3) (results not shown) and 200 μM in rbNaDC1 (*12*). By comparison, the succinate K_{m} measured by radiotracer uptakes is 320 μM in mNaDC1 (*13*) and 450 μM in rbNaDC1 (*16*).

Glutarate-Dependent Currents in Chimeric NaDC1 Transporters. A series of chimeras containing between TM 2 and 10 from mNaDC1 at the N-terminus (shown in Figure 3)

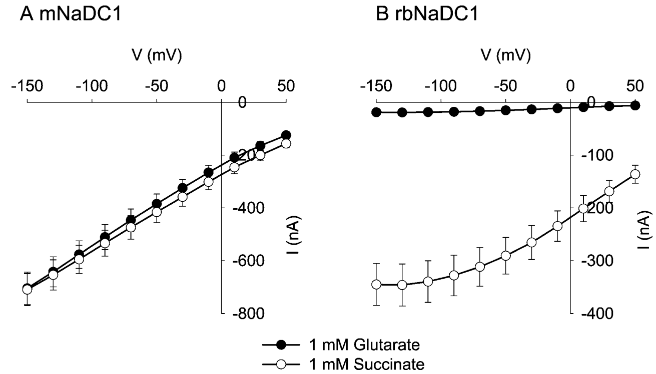

FIGURE 1: Voltage dependence of steady-state substrate-induced currents of wild-type NaDC1 transporters. *Xenopus* oocytes expressing mNaDC1 (A) and rbNaDC1 (B) were superfused with 1 mM succinate or 1 mM glutarate, and the pulse protocol described in Experimental Procedures was followed. The mNaDC1 expressing oocytes exhibited inward currents with both glutarate and succinate, whereas oocytes expressing rbNaDC1 showed voltage-dependent inward currents with succinate but only small currents with glutarate. The data shown are mean ± SEM, n = 18−25 frogs.

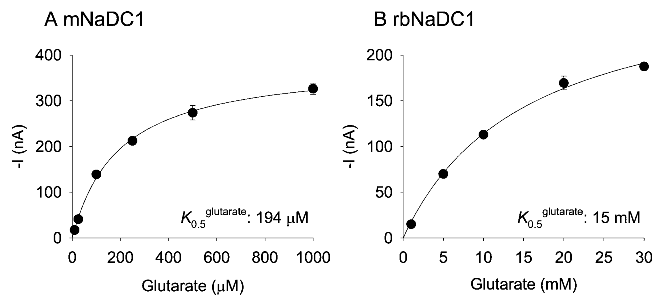

FIGURE 2: Glutarate kinetics in oocytes expressing mNaDC1 (A) and rbNaDC1 (B). Steady-state substrate-dependent currents at −50 mV are shown as a function of different concentrations of glutarate. The figure represents single experiments, and each data point shows mean ± range of duplicate measurements in a single oocyte. The concentrations of glutarate were varied between 10 μM and 1 mM for mNaDC1, and from 1 to 30 mM for rbNaDC1. In mNaDC1, the $K_{0.5}$ for glutarate is 194 μM and $I_{\max}$ is −386 nA. In rbNaDC1, the $K_{0.5}$ is 15.3 mM and the $I_{\max}$ is −289 nA.

was constructed and expressed in *Xenopus* oocytes. The substrate-induced currents were determined as in Figure 1, but only the data from −50 mV are shown. The results are similar at all voltages (results not shown). Most of the chimeras had succinate-induced currents similar to those of the wild-type mouse and rabbit NaDC1, suggesting that the expression of these chimeras is similar to the wild-type proteins (Figure 4). The 2MR chimera exhibited much smaller currents than the wild-type transporters and may be expressed at a lower level. There are no antibodies available against mNaDC1, and therefore, it was not possible to test cell surface expression of the chimeras directly. The series of chimeras with rbNaDC1 at the N-terminus was also constructed and tested, but the activity was too low for further experiments, similar to our previous findings with chimeras between rabbit and human NaDC1 (*9*).

The currents induced by glutarate in mNaDC1 were almost as large as the succinate-induced currents, approximately 92% at −50 mV, whereas in rbNaDC1 the currents with glutarate were approximately 5% of those measured in succinate (Figure 4A, B). The chimeras that contained more TM from mNaDC1 also had increased glutarate-induced currents relative to the succinate-induced currents. There

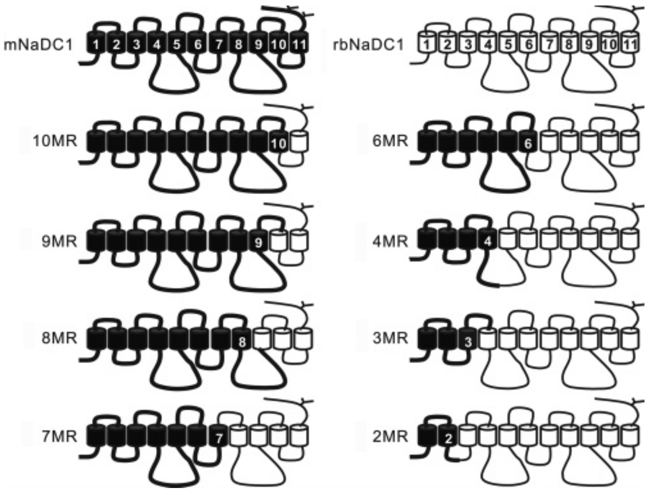

FIGURE 3: Secondary structure models of chimeric NaDC1 transporters used in this study. The cylinders and lines represent predicted transmembrane helices (TM) and associated loops of mouse NaDC1 (filled cylinders, bold lines) and rabbit NaDC1 (unfilled cylinders, narrow lines). The chimeric transporters are designated using the letters M (mouse), R (rabbit), and the number of TM contributed by mNaDC1 at the amino terminus. For example, 2MR contains TM 1−2 from mNaDC1 and 3−11 from rbNaDC1. The junctions to construct the chimeras are located at amino acid positions 74 (2MR), 120 (3MR), 177 (4MR), 284 (6MR), 341 (7MR), 427 (8MR), 489 (9MR), and 518 (10MR) relative to the amino acid sequence of mNaDC1. The Y indicates the *N*-glycosylation site. The extracellular side is at the top of the figure.

were significant differences between the 4MR and 2MR chimeras, the 7MR and 6MR chimeras, and the 8MR and 7MR chimeras (Figure 4B). Therefore, TM 3−4, 7, and 8 contribute to the glutarate-dependent currents, but the largest contribution is made by TM 3−4. The 9MR chimera results were significantly different from wild-type mNaDC1 but not different from the 10MR chimera. Therefore, it is possible that TM 10 is involved in glutarate transport, but the contribution is not large. TM 1, 2, 5, 6, and 11 do not appear to be involved in glutarate transport. The results suggest that the difference between the mouse and rabbit NaDC1 in handling glutarate is determined primarily by residues in TM 3−4 including the associated loop, but other residues in the C-terminal half of the protein also contribute.

Contribution of TM 3−4 to Glutarate-Induced Currents. The R(M3−4) chimera was constructed to investigate further the contribution of TM 3−4 in determining species differences in handling glutarate. The R(M3−4) chimera contains TM 3−4 from mNaDC1, and the rest of the protein is from rbNaDC1 (Figure 5A). The chimeric transporter was expressed in *Xenopus* oocytes, and substrate-dependent currents were measured (Figure 5B). Succinate-induced currents were decreased compared to the wild-type transporters, which may be due to lower expression of the chimeric protein. The glutarate-dependent currents relative to the succinate-evoked currents were 47.5 ± 5.7% ($n = 6$) in the R(M3−4) chimera compared with 5% for rbNaDC1 (Figure 4B), verifying that TM 3 and 4 contribute considerably to glutarate handling in NaDC1. The kinetics of the R(M3−4) chimera with glutarate and succinate were also measured. Substitution of TM 3−4 of mNaDC1 into rbNaDC1 resulted in a large decrease in $K_{0.5}^{\text{glutarate}}$ to 3.6 mM in the experiment shown in Figure 5C and a mean $K_{0.5}^{\text{glutarate}}$ of 4.1 ± 1.1 mM (mean ± SEM, $n = 5$). For comparison, the $K_{0.5}^{\text{glutarate}}$ in rbNaDC1 was 15 mM

Table 1: Comparison of TSR and Free Energy Calculations in Wild-Type rbNaDC1, rbNaDC1 with Single TM Substitutions (TM 3 or 4) and with Double TM Substitution

protein	TSR	$\Delta\Delta G_b$ (kJ/mol)[a]	$\Delta(\Delta\Delta G_b)$ (kJ/mol)[b]
rbNaDC1	0.046 ± 0.001 (5)	7.57	−
R(M3−4)	0.071 ± 0.01* (2)	6.51	−1.07
R(M3)	0.070 ± 0.003* (3)	6.54	−1.03
R(M4)	0.095 ± 0.01* (3)	5.79	−1.78

The numbers in parentheses under TSR values refer to sample size and the * denotes significant difference from wild-type, $p < 0.05$. [a] $\Delta\Delta G_b = -RT \ln(\text{TSR})$. [b] The change in free energy associated with binding glutarate relative to succinate as a result of chimera formation (see Figure 10). $\Delta(\Delta\Delta G_b) = \Delta\Delta G_b(\text{chimera}) - \Delta\Delta G_b(\text{wild-type}) = -RT \ln[(k_{cat}/K_m)_{\text{chimera}}/(k_{cat}/K_m)_{\text{wild-type}}] = -RT \ln[(\text{TSR}_{\text{chimera}})/(\text{TSR}_{\text{wild-type}})]$.

(Figure 2). The R(M3−4) chimera had no change in the $K_{0.5}$ for succinate, 219 ± 29 μM (mean ± range, $n = 2$, results not shown), compared with 203 μM for rbNaDC1 (*12*).

Transport Specificity Ratio (TSR) Analysis of TM 3−4 Chimeras. The results of this study have shown that TM 3 and 4 in NaDC1 are important in determining the $K_{0.5}$ for glutarate. However, the catalytic efficiency of a transporter depends on both $K_{0.5}$ (or K_m) and k_{cat}. In transport experiments, including these, it is often difficult to determine the k_{cat} for lack of a measurement of the amount of transporter protein, or the fraction of that protein that is properly folded and active. The Transport Specificity Ratio (TSR) is a protein-independent constant that reflects a change in substrate specificity for two competing substrates and provides information on the relative catalytic efficiency (*18*) (see Experimental Procedures). Since the TSR calculation is based on initial uptake rates, the time course of uptake of 150 μM ^{14}C-glutarate and 50 μM ^{3}H-succinate was measured between 10 s and 15 min to determine the initial rate of competitive uptake (Figure 6). The time courses were linear at 1 min with both substrates and both transporters; therefore, 1-min uptakes were used for subsequent experiments. The TSR value calculated using 1 min uptakes for mNaDC1 is 0.54 in the experiment shown in Figure 6, compared with a TSR value of 0.043 for rbNaDC1, indicating large differences in catalytic efficiency for glutarate relative to succinate between these two transporters. The mean TSR values are 0.40 ± 0.04 in mNaDC1 and 0.046 ± 0.001 for rbNaDC1 (mean ± SEM, $n = 5$) (Table 1).

Because the TSR value is the ratio of k_{cat}/K_m for the two substrates, we can use the measured $K_{0.5}$ and TSR values to estimate the ratio of k_{cat} for glutarate relative to k_{cat} for succinate ($k_{cat}^{\text{glutarate/succinate}}$). Using the following equation:

$$k_{cat}^{\text{glutarate/succinate}} = \text{TSR}\left[\frac{K_{0.5}^{\text{glutarate}}}{K_{0.5}^{\text{succinate}}}\right] \qquad (5)$$

the $k_{cat}^{\text{glutarate/succinate}}$ for mNaDC1 is 1.03 compared with 3.45 for rbNaDC1. The k_{cat} ratio value in rbNaDC1 implies that the $k_{cat}^{\text{glutarate}}$ is more than 3-fold greater than the $k_{cat}^{\text{succinate}}$. Although somewhat counterintuitive, this could be related to the very low affinity for glutarate in rbNaDC1. Very often in transporters a low substrate affinity is correlated with a high transport capacity, probably a consequence of weaker binding and faster release of the substrate after translocation. Nevertheless, since physiological concentrations of succinate

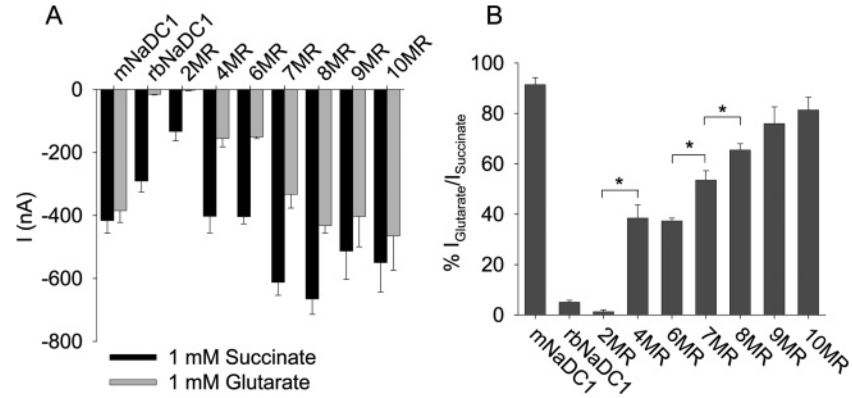

FIGURE 4: Currents in chimeric NaDC1 transporters. (A) Glutarate- and succinate- induced currents at −50 mV in wild type and chimeric NaDC1 transporters. The bars represent mean ± SEM, $n = 25$ (mNaDC1), $n = 18$ (rbNaDC1), $n = 3-10$ (chimeras). The concentration of each substrate was 1 mM. (B) Glutarate-induced currents expressed as a percentage of succinate-induced currents (from A). Asterisks represent $p < 0.05$. In addition, the 9MR chimera is significantly different from mNaDC1.

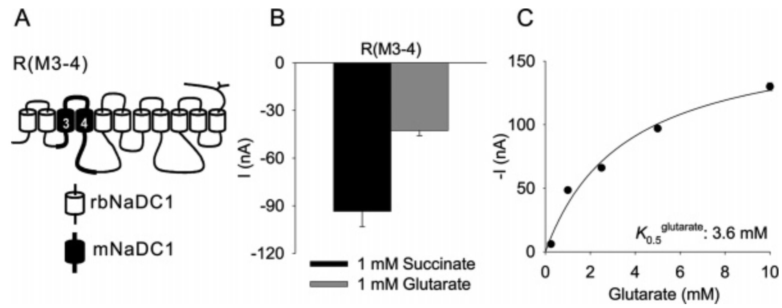

FIGURE 5: Currents in the R(M3−4) chimera. (A) Secondary structure model of the R(M3−4) chimera, containing TM 3−4 and associated loops of mNaDC1 (amino acids 75−177) in rbNaDC1 background. The filled cylinders represent mNaDC1. (B) Currents induced by 1 mM glutarate or succinate in the R(M3−4) chimera, measured at −50 mV. The bars represent mean ± SEM, $n = 6$. (C) Glutarate kinetics in R(M3−4) chimera (same procedure as in Figure 2). The $K_{0.5}^{\text{glutarate}}$ is 3.6 mM and the $I_{\max}$ is −173 nA.

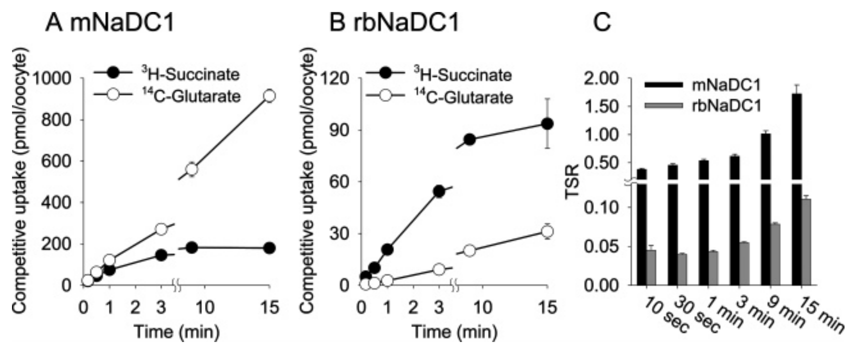

FIGURE 6: Time courses of competitive uptakes in wild-type NaDC1 transporters. Competitive uptakes using oocytes expressing mNaDC1 (A) and rbNaDC1 (B) were measured at different time points, from 10 s to 15 min. The concentrations of ^{14}C-glutarate and ^{3}H-succinate in the transport solution were 150 and 50 μM, respectively. The closed circles represent succinate, and the open circles represent glutarate, mean ± SEM, $n = 5$ oocytes. C, TSR values calculated at different time points for the two wild-type NaDC1 transporters using the data shown in A and B.

and glutarate in plasma are below 20 μM (*21*, *22*), the rabbit NaDC1 functions primarily as a succinate transporter.

We next examined chimeras based on rbNaDC1 containing single or double substitutions of TM 3 or TM 4 from mNaDC1, called R(M3) and R(M4) (Figure 7A). Figure 7B shows competitive uptakes of ^{3}H-succinate and ^{14}C-glutarate in wild-type, single TM substituted chimeras and the double TM substituted chimera, R(M3−4). All three chimeras had measurable uptake activity with glutarate and succinate although the R(M3−4) and R(M3) chimeras exhibited lower activity compared with that of the R(M4) chimera (Figure 7B). The mean TSR values for the chimeras were significantly larger than the TSR value for the wild-type rbNaDC1 (Table 1). For comparison with the wild-type transporters, the $k_{cat}^{\text{glutarate/succinate}}$ ratio is 1.33 in the R(M3−4) chimera.

To determine whether there is functional interaction between TM 3 and 4, we calculated the free energy change ($\Delta(\Delta\Delta G_b)$) produced by each TM substitution (summarized in Table 1). This parameter is an indication of the change in discrimination between the two substrates as a result of the TM substitution. The free energy change of the double TM chimera R(M3−4) is −1.07 kJ/mol compared with the sum of free energies of the two single TM chimeras (R(M3) and R(M4)) of −2.81 kJ/mol (Table 1). The difference in free energy of the double TM chimera is not equal to the sum of the individual TM chimeras; thus, there is likely to be functional interaction between amino acid side chains in TM 3 and 4 (*19*).

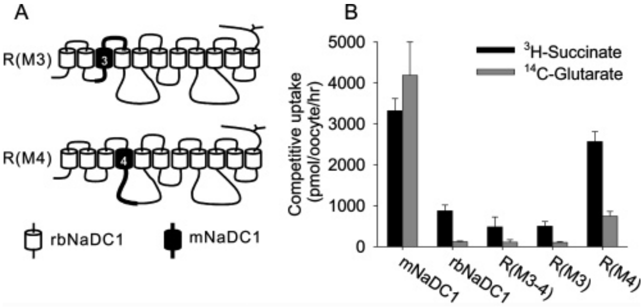

FIGURE 7: Competitive uptake assay in chimeric NaDC1 transporters. (A) Secondary structure models of the R(M3) and R(M4) chimeras containing substitutions of either TM 3 or TM 4 from mNaDC1 (shown by filled cylinders) in rbNaDC1 background. (B) Competitive uptake of glutarate and succinate by wild-type and chimeric NaDC1 transporters expressed in *Xenopus* oocytes. The transport reactions were carried out for 1 min with 150 μM ^{14}C-glutarate and 50 μM ^{3}H-succinate. The bars represent mean ± SEM, $n = 5$ (wild-type), $n = 3$ (R(M3) and R(M4) chimeras), and mean ± range, $n = 2$ (R(M3−4) chimera). TSR values are shown in Table 1.

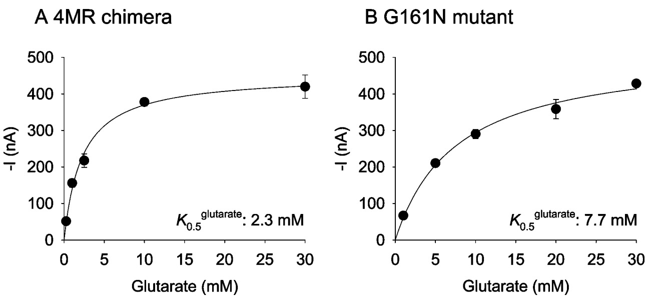

FIGURE 8: Glutarate kinetics in oocytes expressing the 4MR chimera (A) and the G161N mutant (B). Steady-state glutarate-induced currents at −50 mV are shown as a function of different concentrations of the substrate. Each data point shows the mean ± range of duplicate measurements in a single oocyte. The concentrations of glutarate were between 0.25 and 30 mM for 4MR and between 1 and 30 mM for the G161N mutant. In the parental 4MR transporter, the $K_{0.5}^{\mathrm{glutarate}}$ is 2.3 mM, and the $I_{\max}$ is −453 nA. In the G161N mutant, the $K_{0.5}^{\mathrm{glutarate}}$ is 7.7 mM, and the $I_{\max}$ is −520 nA.

Mutants in TM 3−4. To identify the individual amino acids in TM 3 and 4 that determine differences in glutarate $K_{0.5}$ and TSR, site-directed mutagenesis was done using the 4MR chimera as a parental transporter. There are 26 amino acid differences between mouse and rabbit NaDC1 between amino acids 75 and 177 (the TM 3−4 region). In our initial screen, we chose amino acids that are identical between mNaDC1 and mNaDC3, the high affinity transporter that also carries glutarate, but were different from rbNaDC1. These amino acids were mutated from the mNaDC1 sequence to the amino acid found in rbNaDC1 at the same position. The seven mutants were: K77E, C79G, F83L, L149V, G161N, K164S, and D165N. The mutants were first screened for inward currents in the presence of glutarate and succinate. Most did not show any changes, but the G161N mutant appeared to have a decrease in glutarate currents relative to those of succinate (results not shown). In the single experiment shown in Figure 8, the $K_{0.5}^{\mathrm{glutarate}}$ in the G161N mutant was 7.7 mM and $I_{\max}$ was −520 nA, and the $K_{0.5}^{\mathrm{glutarate}}$ in the parental transporter, the 4MR chimera, was 2.3 mM and $I_{\max}$ was −453 nA. In three experiments, the mean $K_{0.5}^{\mathrm{glutarate}}$ in the G161N mutant was 6.1 ± 1.3 mM (mean ± SEM, $n = 3$), significantly different from the $K_{0.5}^{\mathrm{glutarate}}$ of 2.5 ± 0.2 mM ($n = 3$) in the 4MR chimera. However, when we tested TSR values of the mutants, there were no major differences among them or with the 4MR parental transporter (Figure 9). Therefore, Gly-161 appears to be a determinant of binding in the initial Michaelis complex ($K_{0.5}^{\mathrm{glutarate}}$) but not in the transition state complex, which is addressed by the TSR results.

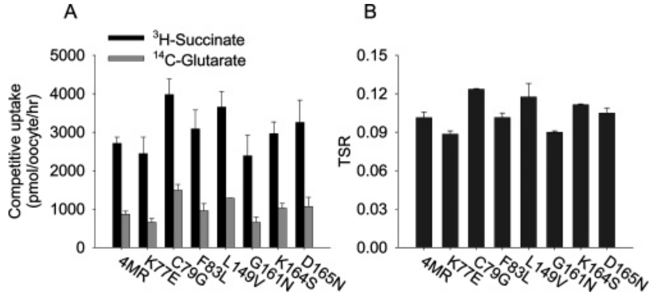

FIGURE 9: Competitive uptake assay in TM 3−4 mutants. (A) Competitive uptake of glutarate and succinate by the TM 3−4 mutants and the 4MR chimera (parental). The transport assay was performed for 1 min with 150 mM ^{14}C-glutarate and 50 mM ^{3}H-succinate. The bars represent mean ± SEM, $n = 6$ for the 4MR chimera, and mean ± range, $n = 2$ for the mutants.

DISCUSSION

This study is based on the observation that the mouse and rabbit NaDC1 orthologs exhibit differences in their handling of glutarate, which differs from succinate by only one carbon. A series of chimeras was made and tested by two-electrode voltage clamp to identify the regions of the protein responsible for transport of glutarate. We found that differences in glutarate transport are determined by residues found throughout the protein, including transmembrane helices (TM) 7, 8 and possibly 10, but the largest contribution is made by TM 3 and 4 and their associated loops. TM 3−4 make significant contributions both to the $K_{0.5}$ for glutarate and to the relative catalytic specificity, measured using the Transport Specificity Ratio (TSR). The results provide evidence of functional coupling between amino acids located in the TM 3−4 region, possibly indicating either a direct interaction between amino acid side chains or cooperative interaction between the amino acids to form a substrate binding site.

Some domains of the NaDC1 protein that affect glutarate transport have been shown in our previous studies to be involved in transport of other substrates. For example, the difference in citrate affinity between the human and rabbit NaDC1 is determined by residues in TM 7, 10, and 11 (*9*). The arginine at position 349, at the extracellular face of TM 7, is required for succinate transport, and the aspartic acid at position 373 in TM 8 is a conformationally sensitive residue (*23*). TM 9−10 appear to form part of the permeation pathway in NaDC1, and this region contains functionally important residues that are alternately accessible and inaccessible to the extracellular medium during the transport cycle (*24*, *25*). Previous studies have also shown that residues that affect the K_m for succinate are also found in TM 1−4, before amino acid 139 (*11*), which corresponds well with the finding in the present study that TM 3−4, including the glycine at position 161, are important in determining the $K_{0.5}$ for glutarate.

Transport specificity ratio (TSR) analysis provides information on changes in catalytic efficiency with glutarate and

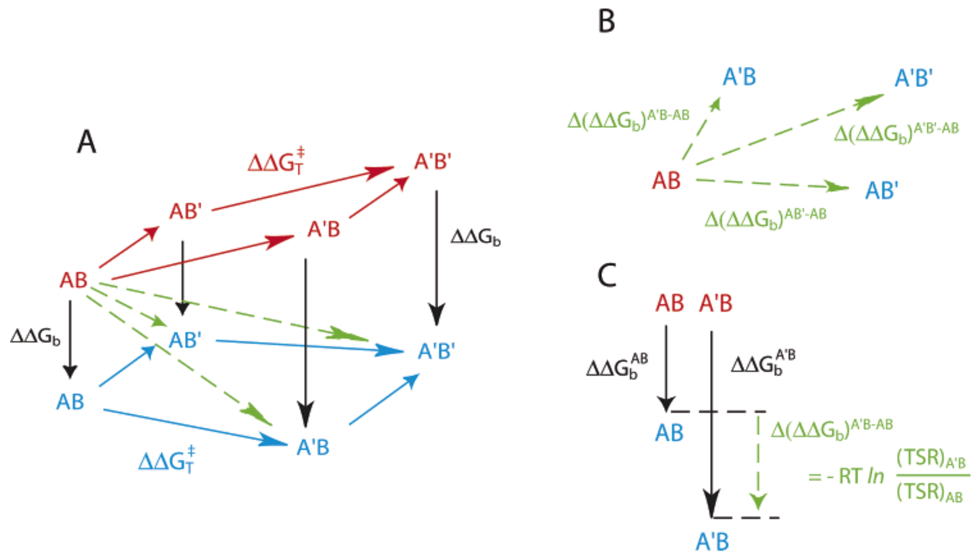

FIGURE 10: TSR analysis of double-mutant cycles. Double-mutant cycles featuring two chimeric constructs (A′ and B′) are shown operating with two substrates, one shown in red and the other in blue. Each corner of the resulting thermodynamic cube (Panel A) is a binding energy (ΔG_b) used in transition-state stabilization. Free energy changes along the black arrows are due to differences in substrate structure, and are given directly by the measured TSR parameter ($\Delta\Delta G_b$, eq 3). Free energy changes along the red or blue arrows represent changes in the transition-state stabilization energy ($\Delta\Delta G_T^{\ddagger}$) with a single substrate that are due to changes in the protein as a result of chimera formation (*19*). Free energy changes along vertical diagonals (green dash arrows) represent changes in the TSR parameter ($\Delta\Delta G_b$) that are due to changes in chimeric structure. (B) Free energy changes along vertical diagonals (green dash arrows) in the thermodynamic cube (Panel A) are shown here as a flattened two-dimensional representation. Each of these arrows represents the difference in discriminating between two substrates as a result of forming the single chimeras (A′B or AB′), or the double chimera (A′B′) compared with the wild-type protein (AB). If the magnitude of the longer arrow (in Panel A) is equal to the magnitude of the sum of the two shorter arrows, the changes in free energy as a result of chimera formation are independent of one another. This simple additive relationship fails, however, when there is "interaction" or "coupling" between chimeric structures A′ and B′. Thus, formally, the condition: $\Delta(\Delta\Delta G_b)A'B' = \Delta(\Delta\Delta G_b)A'B + \Delta(\Delta\Delta G_b)AB' + \Delta\Delta G_{T(I)}^{\ddagger}$ indicates the presence of an interaction if there is a nonzero value of $\Delta\Delta G_{T(I)}^{\ddagger}$, the "transition-state interaction energy" (*19*). Panel C shows the example for chimera A′B, which compares the $\Delta\Delta G_b$ of AB (wild-type) to that measured for one of the three chimeric forms A′B. The equation in green font is a function of the logarithm of the indicated ratios, which take the form, $TSR_{chimera}/TSR_{wild-type}$ (see Table 1 calculations). This equation states in mathematical terms that the thermodynamic length of the green arrow is equal to the difference between the black arrow lengths, which are measured by TSR analysis (eq 3).

succinate as a consequence of chimera formation (*26*). The mouse and rabbit NaDC1 transporters differ in their TSR values by more than 10-fold, reflecting the large differences in substrate specificity of glutarate relative to succinate. Since the TSR is based on a change in free energy of transition-state binding for two competitive substrates, $\Delta\Delta G_b$, the TSR measurement can be used to estimate the effect of a mutation or chimera on the relative heights of the translocation energy barrier for the two substrates. Previous studies have shown that changes in free energy of single and double mutants relative to the wild-type proteins can provide information on whether the mutated amino acids interact in the transition state (*19*). If two residues are not close to one another and not functionally coupled, then the sum of changes in transition-state stabilization energy for two individual mutations is equal to that for the corresponding double mutations (*19*). However, a difference between the sum of changes in free energy of two single mutations compared with the double mutant indicates that the mutations alter the interactions between these residues. TSR analysis is somewhat more complex because two substrates are involved (summarized in Figure 10). However, adaptation of these principles to the particular circumstances of TSR analysis leads to the conclusion that there is transition-state interaction energy between TM 3 and 4, and this interaction has a functional role in determining the relative specificities for glutarate versus succinate. Our single and double chimeras exhibit nonadditivity since the sum of $\Delta(\Delta\Delta G_b)$ for the two single TM chimeras (−2.81 kJ/mol) is not the same as that for the chimera containing both TM 3 and 4 (−1.07 kJ/mol) (Table 1). This suggests that the function of TM 3 is coupled with that of TM 4 in the transition state. In other studies, a similar difference between the free energy changes of single and double mutants was found for polar residues in TM 4 and 5 of the dopamine transporter, suggesting the residues interact in the initial Michaelis complex (*27*).

The amino acids responsible for differences in glutarate handling in NaDC1 appear to be distributed throughout the protein, with contributions from TM 7, 8, and possibly 10 adding to the effects of TM 3−4. This indicates that amino acids found on multiple helical surfaces contribute to transport of glutarate in NaDC1, which is in agreement with other studies of transport proteins. For example, the affinity for glucose in the facilitative glucose transporters Hxt1 and Hxt2 from *Saccharomyces cerevisiae* is determined by at least four amino acids found in TM 1, 5, 7, and 8 (*28*). In the mammalian facilitative glucose transporters, glucose affinity is determined by residues in TM 9−12, whereas TM 1−2 and 6−11 contain determinants of fructose transport (*29*, *30*). In addition, amino acids in TM 7 and 2 in GLUT7 appear to form a selectivity filter that restricts access of some substrates to the substrate binding site (*31*). Crystal structures of transport proteins, such as the recent structures of the bacterial Na^+/Cl^--dependent leucine transporter and the lactose permease, show that substrate binding sites are within hydrophilic cavities formed by multiple helices (*32*, *33*).

The differences between rabbit and mouse NaDC1 in handling glutarate are more likely related to differences in transition state rather than the initial binding of substrate to the transporter. In transporters, the substrate specificity (k_{cat}/K_m) or the ability to discriminate between two substrates depends on the height of the activation energy barrier (*18*). As shown by the differences in TSR values, mNaDC1 has very similar transition-state stabilization (small $\Delta\Delta G_b$) for glutarate and succinate, which limits discrimination between them. In contrast, rbNaDC1 does a better job of discriminating between the two substrates, and this is reflected in the larger difference in binding energy used for transition-state stabilization. The best fit to the substrate is most likely during the transition-state complex (*34*), and the observed differences between the transporters could reflect differences in accommodating the two substrates in the transition state. For example, the mNaDC1 protein could be more flexible to orient the critical residues in the protein with substrates of different structures.

In conclusion, the mouse and rabbit NaDC1 exhibit differences in handling the five-carbon dicarboxylate, glutarate. The mNaDC1 exhibits substrate-dependent currents with glutarate as large as those with succinate, and the TSR value of 0.4 reflects a relatively high efficiency of transporting glutarate relative to succinate. The rbNaDC1 has only small currents in the presence of glutarate and a succinate affinity similar to that of mNaDC1, reflected in a very low TSR value of 0.046. The results of this study show that the differences in glutarate transport are determined primarily by the interaction of multiple amino acids found in TM 3 and 4, with contributions from TM 7, 8, and 10 or the associated loops. TM 3−4 make important contributions to substrate affinity and specificity in NaDC1. Furthermore, we find evidence of functional coupling between amino acids in TM 3 and TM 4.

ACKNOWLEDGMENT

Many thanks to Dr. James C. Lee for providing valuable insights into intramolecular interaction between transmembrane helices. We also thank Dr. Bert X. Yao for his participation in making the initial set of chimeras and Kathleen Randolph for her assistance in preparation of solutions.

REFERENCES

1. Pajor, A. M. (2006) Molecular properties of the SLC13 family of dicarboxylate and sulfate transporters, *Pflugers Arch. 451*, 597−605.
2. Pajor, A. M. (2000) Molecular properties of sodium/dicarboxylate cotransporters, *J. Membr. Biol. 175*, 1−8.
3. Dantzler, W. H. and Evans, K. K. (1996) Effect of αKG in lumen on PAH transport by isolated perfused proximal tubules, *Am. J. Physiol. 271*, F521−F526.
4. Pak, C. Y. C. (1991) Etiology and treatment of urolithiasis, *Am. J. Kidney Diseases 18*, 624−637.
5. Rogina, B., Reenan, R. A., Nilsen, S. P., and Helfand, S. L. (2000) Extended life-span conferred by cotransporter gene mutations in *Drosophila*, *Science 290*, 2137−2140.
6. Fei, Y. J., Inoue, K., and Ganapathy, V. (2003) Structural and functional characteristics of two sodium-coupled dicarboxylate transporters (ceNaDC1 and ceNaDC2) from *Caenorhabditis elegans* and their relevance to life span, *J. Biol. Chem. 278*, 6136−6144.
7. Pajor, A. M., and Sun, N. (1996) Characterization of the rabbit renal Na^+-dicarboxylate cotransporter using antifusion protein antibodies, *Am. J. Physiol. 271*, C1808−C1816.
8. Zhang, F. F., and Pajor, A. M. (2001) Topology of the Na^+/dicarboxylate cotransporter: the N-terminus and hydrophilic loop 4 are located intracellularly, *Biochim. Biophys. Acta 1511*, 80−89.
9. Kahn, E. S., and Pajor, A. M. (1999) Determinants of substrate and cation affinities in the Na^+/dicarboxylate cotransporter, *Biochemistry 38*, 6151−6156.
10. Pajor, A. M., Kahn, E. S., and Gangula, R. (2000) Role of cationic amino acids in the Na^+/dicarboxylate co-transporter NaDC-1, *Biochem. J. 350*, 677−683.
11. Pajor, A. M., Sun, N., Bai, L., Markovich, D., and Sule, P. (1998) The substrate recognition domain in the Na^+/dicarboxylate and Na^+/sulfate cotransporters is located in the carboxy-terminal portion of the protein, *Biochim. Biophys. Acta 1370*, 98−106.
12. Pajor, A. M., Hirayama, B. A., and Loo, D. D. F. (1998) Sodium and lithium interactions with the Na^+/dicarboxylate cotransporter, *J. Biol. Chem. 273*, 18923−18929.
13. Pajor, A. M., and Sun, N. N. (2000) Molecular cloning, chromosomal organization, and functional characterization of a sodium-dicarboxylate cotransporter from mouse kidney, *Am. J. Physiol. Renal Physiol. 279*, F482−F490.
14. Burckhardt, B. C., Lorenz, J., Kobbe, C., and Burckhardt, G. (2005) Substrate specificity of the human renal sodium dicarboxylate cotransporter, hNaDC-3, under voltage-clamp conditions, *Am. J. Physiol. Renal Physiol. 288*, F792−F799.
15. Kunkel, T. A. (1985) Rapid and efficient site-specific mutagenesis without phenotypic selection, *Proc. Natl. Acad. Sci. U.S.A. 82*, 488−492.
16. Pajor, A. M. (1995) Sequence and functional characterization of a renal sodium/dicarboxylate cotransporter, *J. Biol. Chem. 270*, 5779−5785.
17. Yao, X., and Pajor, A. M. (2000) The transport properties of the human renal Na^+/dicarboxylate cotransporter under voltage clamp conditions, *Am. J. Physiol. 279*, F54−F64.
18. King, S. C. (2004) The "Transport Specificity Ratio": a structure−function tool to search the protein fold for loci that control transition-state stability in membrane transport catalysis, *BMC Biochem. 5*, 16.
19. Wells, J. A. (1990) Additivity of mutational effects in proteins, *Biochemistry 29*, 8509−8517.
20. Pajor, A. M., and Sun, N. (1996) Functional differences between rabbit and human Na^+-dicarboxylate cotransporters, NaDC-1 and hNaDC-1, *Am. J. Physiol. 271*, F1093−F1099.
21. Baric, I., Wagner, L., Feyh, P., Liesert, M., Buckel, W., and Hoffmann, G. F. (1999) Sensitivity and specificity of free and total glutaric acid and 3-hydroxyglutaric acid measurements by stable-isotope dilution assays for the diagnosis of glutaric aciduria type I, *J. Inherited Metab. Dis. 22*, 867−881.
22. Kushnir, M. M., Komaromy-Hiller, G., Shushan, B., Urry, F. M., and Roberts, W. L. (2001) Analysis of dicarboxylic acids by tandem mass spectrometry. High-throughput quantitative measurement of methylmalonic acid in serum, plasma, and urine, *Clin. Chem. 47*, 1993−2002.
23. Yao, X., and Pajor, A. M. (2002) Arginine-349 and aspartate-373 of the Na^+/dicarboxylate cotransporter are conformationally sensitive residues, *Biochemistry 41*, 1083−1090.
24. Pajor, A. M. (2001) Conformationally sensitive residues in transmembrane domain 9 of the Na^+/dicarboxylate co-transporter, *J. Biol. Chem. 276*, 29961−29968.
25. Pajor, A. M., and Randolph, K. M. (2005) Conformationally sensitive residues in extracellular loop 5 of the Na^+/dicarboxylate co-transporter, *J. Biol. Chem. 280*, 18728−18735.
26. King, S. C., Hu, L. A., and Pugh, A. (2003) Induction of substrate specificity shifts by placement of alanine insertions within the consensus amphipathic region of the *Escherichia coli* GABA (γ-aminobutyric acid) transporter encoded by GabP, *Biochem. J. 376*, 645−653.
27. Itokawa, M., Lin, Z., Cai, N. S., Wu, C., Kitayama, S., Wang, J. B., and Uhl, G. R. (2000) Dopamine transporter transmembrane domain polar mutants: ΔG and $\Delta\Delta G$ values implicate regions important for transporter functions, *Mol. Pharmacol. 57*, 1093−1103.
28. Kasahara, T., and Kasahara, M. (2003) Transmembrane segments 1, 5, 7 and 8 are required for high-affinity glucose transport by *Saccharomyces cerevisiae* Hxt2 transporter, *Biochem. J. 372*, 247−252.

29. Buchs, A. E., Sasson, S., Joost, H. G., and Cerasi, E. (1998) Characterization of GLUT5 domains responsible for fructose transport, *Endocrinology 139*, 827−831.

30. Wu, L., Fritz, J. D., and Powers, A. C. (1998) Different functional domains of GLUT2 glucose transporter are required for glucose affinity and substrate specificity, *Endocrinology 139*, 4205−4212.

31. Manolescu, A., Salas-Burgos, A. M., Fischbarg, J., and Cheeseman, C. I. (2005) Identification of a hydrophobic residue as a key determinant of fructose transport by the facilitative hexose transporter SLC2A7(GLUT7), *J. Biol. Chem. 280*, 42978−42983.

32. Yamashita, A., Singh, S. K., Kawate, T., Jin, Y., and Gouaux, E. (2005) Crystal structure of a bacterial homologue of Na^+/Cl^--dependent neurotransmitter transporters, *Nature 437*, 215−223.

33. Abramson, J., Smirnova, I., Kasho, V., Verner, G., Kaback, H. R., and Iwata, S. (2003) Structure and mechanism of the lactose permease of *Escherichia coli*, *Science 301*, 610−615.

34. Klingenberg, M. (2005) Ligand-protein interaction in biomembrane carriers. The induced transition fit of transport catalysis, *Biochemistry 44*, 8563−8570.

BI052328G